APPLIED PHYSICS LETTERS **98**, 264104 (2011)

Shear-enhanced adhesiveless transfer printing for use in deterministic materials assembly

Andrew Carlson,[1] Hyun-Joon Kim-Lee,[2] Jian Wu,[3] Paulius Elvikis,[4] Huanyu Cheng,[3] Anton Kovalsky,[1] Steven Elgan,[4] Qingmin Yu,[3,5] Placid M. Ferreira,[4] Yonggang Huang,[3] Kevin T. Turner,[2,a)] and John A. Rogers[1,a)]

[1]*Department of Materials Science and Engineering, Beckman Institute, and Frederick Seitz Materials Research Laboratory, University of Illinois at Urbana-Champaign, Illinois 61801, USA*
[2]*Department of Mechanical Engineering, University of Wisconsin-Madison, Wisconsin 53706, USA*
[3]*Department of Civil and Environmental Engineering, and Department of Mechanical Engineering, Northwestern University, Illinois 60208, USA*
[4]*Department of Mechanical Science and Engineering, University of Illinois at Urbana-Champaign, Illinois 61801, USA*
[5]*School of Mechanics, Civil Engineering and Architecture, Northwestern Polytechnical University, Xi'an 710072, People's Republic of China*

(Received 21 March 2011; accepted 7 June 2011; published online 28 June 2011)

This letter describes the physics and application of an approach to transfer printing that utilizes targeted shear loading to modulate stamp adhesion in a controlled and repeatable fashion. Experimental measurements of pull-off forces as functions of shear and stamp dimension reveal key scaling properties and provide a means for comparison to theory and modeling. Examples of printed structures in suspended and multilayer configurations demonstrate some capabilities in micro/nanoscale materials assembly. © *2011 American Institute of Physics*. [doi:10.1063/1.3605558]

Transfer printing is a technique for assembling solid material structures (e.g., semiconductor microdevices, carbon nanotubes, and others) onto unusual substrates for use in types of flexible electronic and optoelectronic devices.[1–6] In its most versatile form, the adhesion to the surface of an elastomeric stamp is modulated through peeling velocity, where high and low peel rates correspond to modes for retrieval (i.e., lifting objects from a source substrate) and delivery (i.e., printing these objects onto a receiver), respectively.[7,8] For efficient delivery, the relative adhesive strength at the interface between the objects (i.e., inks) and the stamp must be less than that between the objects and receiver.[7–9] Advanced printing modalities can reduce the adhesion at the stamp/ink interface to levels below that of the slow peel limit, but they typically require stamps with complex surface relief and/or mechanical loading protocols.[9,10] Studies in other contexts show that directional shearing at an interface can control the behavior in a variety of micro- and nanostructured dry adhesives.[11–15] Here, release occurs when applied shear loads mechanically initiate separation or alter interface loading at the adhesive surface.[12,13,15] Here, we explore different, but related, ideas to achieve shear-assisted transfer printing with simple, flat stamps. Analytical and finite element modeling results coupled with printing demonstrations reveal the underlying mechanics of this process and the resulting capabilities in materials assembly.

Fig. 1(a) presents a schematic illustration of shear-assisted printing with an elastomeric stamp comprising a single, rectangular post mounted to a thick backing layer (950 μm, inset, Fig. 1(a)). Lateral post dimensions directly match the underlying ink, here illustrated as a green plate.[1,16,17] During retrieval, the stamp is conformally contacted to the ink, then rapidly retracted to maximize adhesion through viscoelastic effects.[7,8] To print, the inked stamp is placed in contact with a receiver substrate. The receiver is then displaced laterally (through motion of the underlying stage) and the stamp slowly delaminated. This displacement generates a shear deformation in the stamp that reduces the normal component of the force required to induce delamination, facilitating efficient release of the ink onto the receiver. Fig. 1(b) provides plan view optical images from a shear-assisted printing event highlighting contact, shearing, and release between a poly(dimethylsiloxane) (PDMS, 5:1

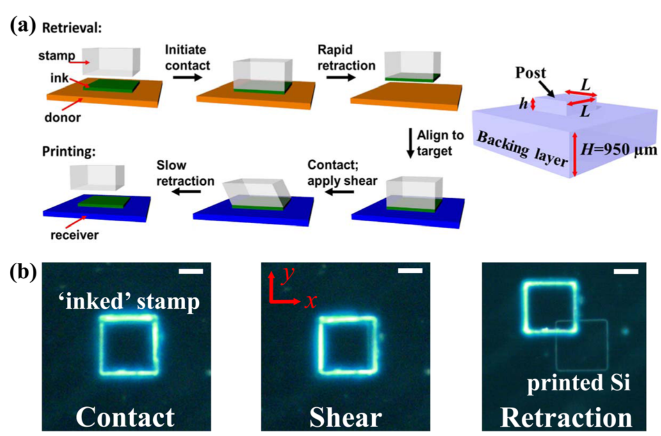

FIG. 1. (Color online) (a) Steps for transfer printing with an elastomeric stamp, where applied shear stresses are used to control the strength of adhesion. Inset: a schematic illustration and critical dimensions of the stamp including post and backing layer. (b) Optical micrographs collected by imaging through the transparent stamp during the printing steps. A stamp "inked" with a silicon plate ($100 \times 100 \times 3$ μm) is brought into contact with a silicon substrate, sheared by 12.5 μm ($\gamma = 14\%$) in the -x-direction, and then slowly retracted to transfer the plate from stamp to substrate. Scale bars correspond to 50 μm.

[a)]Authors to whom correspondence should be addressed. Electronic addresses: kturner@engr.wisc.edu and jrogers@illinois.edu.

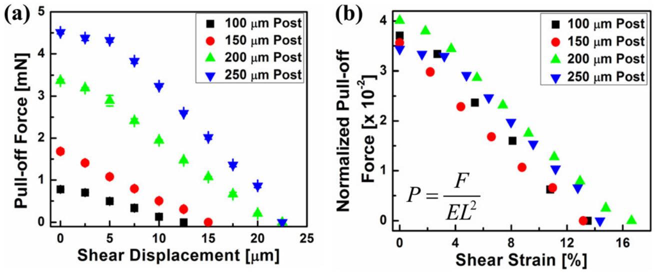

FIG. 2. (Color online) (a) Measured pull-off forces required to delaminate stamps from a flat silicon substrate, as a function of shear displacement. The posts on the stamps have fixed heights of 50 μm and lateral dimensions up to 250 μm; retraction and shear velocities were fixed at 10 μm/s. (b) Normalized pull-off forces, P, from (a) as a function of shear strain (from Eq. (1)) in the post. The data from posts with different sizes collapse, approximately, onto a single line.

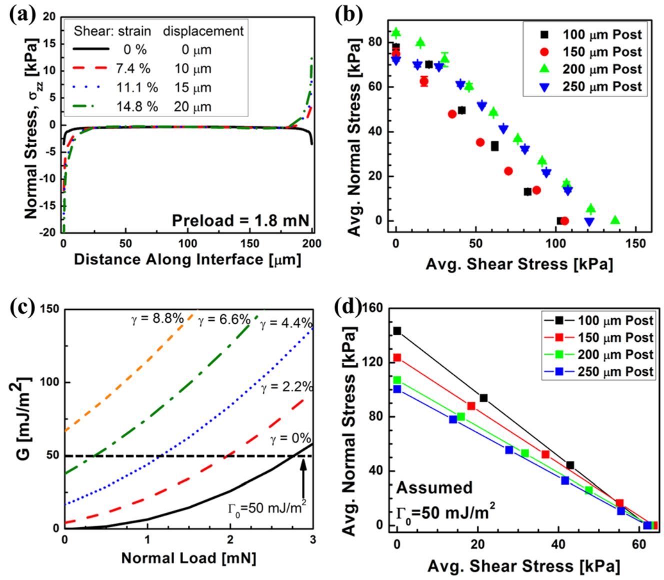

FIG. 3. (Color online) (a) Calculated normal stress distributions in a 200 μm wide post 1 μm above the stamp-ink interface for shear strains between 0% and 14.8%. (b) Average normal stress as a function of average shear stress at the interface for the pull-off forces in Figure 2. The stresses were determined from measured loads and applied shear displacements using a finite element model. The data collapse onto approximately a single line. (c) Strain energy release rate, G, calculated using finite element analysis, for a stamp with a post width $L = 150$ μm at different applied shear strains and normal forces. The pull-off force at failure can be determined from the intersection of the curves with the toughness of the interface (black dashed line shows a representative toughness of $\Gamma_0 = 50$ mJ/m^2). (d) Average normal stress vs. average shear stress at failure of the stamp/Si interface predicted from fracture-based finite element calculations assuming $\Gamma_0 = 50$ mJ/m^2. Modeling results exhibit similar behavior to the experimental results in (b).

monomer:catalyst mix ratio) stamp ($100 \times 100 \times 50$ μm), a monocrystalline silicon ink ($100 \times 100 \times 3$ μm), and a silicon wafer substrate.

Shear loads can generate mixed-mode loading at interfaces, in a way that influences the failure behavior.[18,19] Remote application of shear force can also affect the overall stress distribution at the interface. To evaluate stamp adhesion under various shear loading, normal direction pull-off forces were measured using a custom setup (see supplementary information).[10,20] Single-post PDMS stamps fabricated via casting and curing techniques,[9,10] with lateral dimensions ranging from 100 μm to 250 μm, were mounted to motorized x, y, z stages and a precision load cell (Transducer Techniques, GSO-10) to measure forces in the z-direction. Lateral displacement of the stage in x followed by retraction of the stamp in z provided force-displacement curves (see supplementary information[20]) from which pull-off forces, F, could be determined. Fig. 2(a) shows a characteristic decrease in adhesion with increasing shear displacement, u, for four different post sizes. Here, the velocities for shearing and retracting were fixed at 10 μm/s. When forces are normalized as $P = F/(EL^2)$ and u converted to shear strain γ (Eq. (1) below), the measurements from stamps with different lateral dimensions all exhibit similar behavior (Fig. 2(b)). In these calculations, E is the Young's modulus, taken as E = 2.1 MPa, L is the lateral dimension of the post, and ν is the Poisson's ratio, $\nu = 0.49$.[7,10] Similar trends are evident for other shear and delamination velocities (see supplementary information[20]).

The shear strain in the post γ is determined from the shear displacement and stamp geometry through a mechanics analysis that accounts for the compliance of the backing layer which is wider and thicker than the post and modeled as a semi-infinite solid. Setting a coordinate system origin at the bottom center of the post with x, z axes pointing to the shear and stamp height directions, respectively, a concentrated shear force Q applied at this origin causes displacement w of $w = \frac{Q}{2\pi\mu\sqrt{x^2+y^2}}\left(1 - \nu + \nu\frac{x^2}{x^2+y^2}\right)$,[21] where μ is the shear modulus of the stamp. For a uniform shear stress τ applied to an $L \times L$ post, the average displacement $\bar{u}$ along the shear direction is obtained by integrating the above expression, $\bar{u} = (2-\nu)\tau L \ln(\sqrt{2}+1)/(\pi\mu)$. Defining post shear strain as $\gamma = \tau/\mu$, and recognizing that the measured shear displacement u is the sum of $\bar{u}$ and γh, where h is the height of the post, yields the shear strain in the post,

$$\gamma = \frac{u}{h + (2-\nu)\ln(\sqrt{2}+1)\frac{L}{\pi}}. \qquad (1)$$

To further understand the experimental results, a 3-D finite element (FE) model of the post-ink system was developed for the full stamp geometry. Using the FE model with the applied shear displacements and measured pull-off forces as inputs, the average normal and shear stresses on the posts at failure were calculated (Fig. 3(b)) and the data from multiple posts of different widths collapse to a single line. This result shows that the average normal stress at failure decreases with increasing shear while demonstrating the validity of the analytical shear strain expression. Under pure normal loading, the normal stress distribution in the post just above the stamp-ink interface is symmetric with stress concentrations at the edges (black line, Fig. 3(a)). As shear displacement is applied, the stress distribution becomes asymmetric and produces a larger normal stress at the trailing edge (dotted lines, Fig. 3(a)). This change arises because the shear force is applied above the interface and thus generates a moment on the interface. This moment and the asymmetric stress distribution that it induces is the key reason that the pull-off force is reduced with applied shear. Similar moments generated by the shear have previously been used to explain the stick-slip motion of an elastic block.[22]

To allow quantitative analysis, an initial crack, 200 nm in length, is incorporated in the FE model at the edge of post/ink interface, and the strain energy release rate is calculated using the virtual crack closure technique (VCCT).[23] While the assumed initial crack length here is arbitrary as it cannot be measured directly in experiments, the calculations are expected to be able to capture the overall trend of the data. The strain energy release rate, G, for a post of width $L = 150\ \mu$m is plotted as a function of applied normal force and shear strain in Fig. 3(c). Assuming a Griffith fracture criterion, the crack will propagate when $G > \Gamma_0$, where Γ_0 is the interface toughness; a representative PDMS-Si toughness of 50 mJ/m^2 is shown in Fig. 3(c). The results illustrate that the failure criterion is reached at lower normal forces with increasing applied shear strain. Fig. 3(d) shows the combination of normal stress and shear stress to satisfy the fracture criterion with $\Gamma_0 = 50$ mJ/m^2 for posts with $L = 100$, 150, 200, and 250 μm. The FE predictions in Fig. 3(d) exhibit a similar trend to the experimental results in Fig. 2(b). While the overall behavior is similar, the slope of the critical normal-shear stress boundary predicted by the model is steeper than that observed in the experiments. This difference is likely due to the assumptions (e.g., initial crack length, interface toughness, perfect alignment, and lateral stiffness of the measurement setup) and simplifications (e.g., simple fracture criterion and linear elasticity of PDMS) made in the model. Nevertheless, these modeling results effectively demonstrate the mechanism by which the applied shear displacement reduces the normal pull-off force in shear assisted transfer printing.

Fig. 4(a) provides a relationship between the applied shear strain and yields for silicon plates printed onto the bare surface of a silicon wafer. Procedures for fabrication of the inks are similar to methods described previously.[10,20,24,25] A $\sim 10\times$ enhancement in yield is observed for a shear strain of 14%; statistics were based on 60 prints at each strain value. These improvements expand the capabilities of transfer printing to allow delivery of inks onto otherwise challenging receiver substrates. An example of a textured surface appears in Fig. 4(b), where the relief consists of lines and spaces (3 μm width, 17 μm spacing) molded onto the surface of a PDMS substrate (2:1 monomer:catalyst mixing ratio). The contact area here corresponds to <15% of the area of the ink, thereby providing adhesion that would be too low to enable printing with previously reported peel-rate control strategies. Freely suspended structures and multilevel arrangements of inks, such as the collection of overhanging and stacked plates printed onto silicon substrates in Figs. 4(c) and 4(d), respectively, represent some other assembly examples enabled by shear. The versatility of this technique and its compatibility with semiconductor and other classes of micro/nanoscale inks could provide means to fabricate unusual microelectromechanical systems and device structures in electronics, optoelectronics, and other areas of interest.

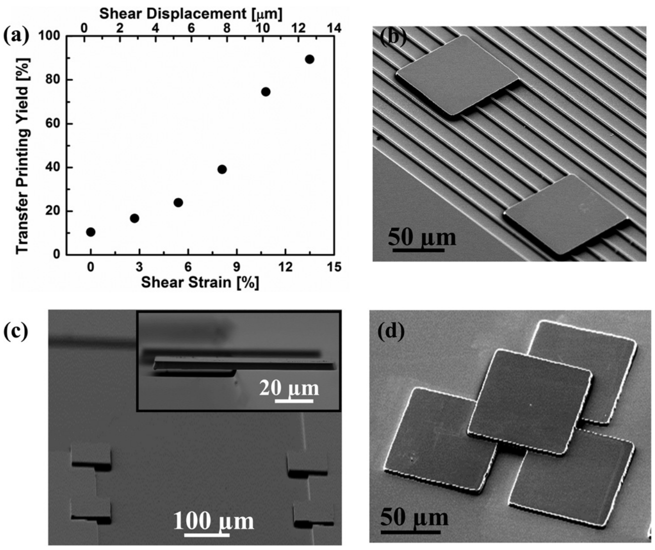

FIG. 4. Demonstrations of printing silicon plates ($100 \times 100 \times 3\ \mu$m) using shear to control the adhesion. (a) Yields for transfer printing onto a bare silicon substrate as a function of shear. (b) Examples of plates printed onto a structured (line and space geometry; 3 μm width, 17 μm spacing) PDMS substrate. (c) Plates printed onto a micromachined ledge on a silicon wafer. Inset: cross-sectional magnified view. (d) Overlapping, stacked plates printed onto a silicon wafer surface.

We thank T. Banks and B. Sankaran for assistance with processing using facilities at the Frederick Seitz Materials Research Laboratory (MRL). The general characterization facilities were provided through MRL with support from the University of Illinois and from DOE Grant Nos. DE-FG02-07ER46453 and DE-FG02-07ER46471. A.C. acknowledges support from the National Defense Science and Engineering Graduate (NDSEG) Fellowship program. K.T.T. and H.J.K. acknowledge support through AFOSR-MURI FA9550-08-1-0337 and NSF Grant No. CMMI-#0845294.

[1] J.-H. Ahn *et al.*, Science **314**, 1754 (2006).
[2] Q. Cao *et al.*, Nature **454**, 495 (2008).
[3] D.-H. Kim *et al.*, Science **320**, 507 (2008).
[4] S.-I. Park *et al.*, Science **325**, 977 (2009).
[5] J. Viventi *et al.*, Sci. Transl. Med. **2**, 24ra22 (2010).
[6] J. Yoon *et al.*, Nat. Mater. **7**, 907 (2008).
[7] X. Feng *et al.*, Langmuir **23**, 12555 (2007).
[8] M. A. Meitl *et al.*, Nat. Mater. **5**, 33 (2006).
[9] T.-H. Kim *et al.*, Appl. Phys. Lett. **94**, 113502 (2009).
[10] S. Kim *et al.*, Proc. Natl. Acad. Sci. U.S.A. **107**, 17095 (2010).
[11] B. Aksak, M. P. Murphy, and M. Sitti, in *Proceedings of the 2008 IEEE International Conference on Robotics and Automation* (IEEE, Pasadena, 2008) p. 3058.
[12] M. Murphy, B. Aksak, and M. Sitti, Small **5**, 170 (2009).
[13] R. K. Kramer, C. Majidi, and R. J. Wood, Adv. Mater. **22**, 3700 (2010).
[14] M. Varenberg, and S. Gorb, J. R. Soc., Interface **4**, 721 (2007).
[15] H. E. Jeong *et al.*, Proc. Natl. Acad. Sci. U.S.A. **106**, 5639 (2009).
[16] K. J. Lee *et al.*, J. Micromech. Microeng. **20**, 075018 (2010).
[17] A. J. Baca *et al.*, Adv. Funct. Mater. **17**, 3051 (2007).
[18] J. Dundurs, J. Appl. Mech. **36**, 650 (1969).
[19] J. Hutchinson and Z. Suo, Adv. Appl. Mech. **29**, 63 (1992).
[20] See EPAPS supplementary material at http://dx.doi.org/0.1063/1.3605558 for information on evaluation of shear-assisted transfer printing.
[21] L. D. Landau, and E. M. Lifshitz, *Theory of Elasticity*, 3rd ed. (Butterworth Heinermann, Oxford, 1986).
[22] J. Scheibert and D. K. Dysthe, Europhys. Lett. **29**, 54001 (2010).
[23] R. Krueger, Appl. Mech. Rev. **57**, 109 (2004).
[24] Y. Yang *et al.*, Small **7**, 484 (2011).
[25] M. A. Meitl *et al.*, Appl. Phys. Lett. **90**, 083110 (2007).